Article:
Fang, Y, Cui, J, Wanatowski, D et al. (2022) Subsurface settlements of shield tunneling predicted by 2D and 3D constitutive models considering non-coaxiality and soil anisotropy: a case study. Canadian Geotechnical Journal, 59 (3). pp. 424-440. ISSN: 0008-3674

https://doi.org/10.1139/cgj-2020-0620

Subsurface settlements of shield tunneling predicted by 2D and 3D constitutive models considering non-coaxiality and soil anisotropy: a case study

Yong Fang[a], Jian Cui[a], Dariusz Wanatowski[d], Nikolaos Nikitas[d], Ran Yuan[b], Yi He[bc]*

[a] Key Laboratory of Transportation Tunnel Engineering, Ministry of Education, Southwest Jiaotong University, Chengdu 610031, China

[b] Key Laboratory of High-speed Railway Engineering, Ministry of Education, Southwest Jiaotong University, Chengdu 610031, China

[c] Faculty of Geosciences and Environmental Engineering, Southwest Jiaotong University, Chengdu 610031, China

[d] School of Civil Engineering, University of Leeds, Leeds LS2 9JT, UK

Yi He is the **corresponding author**.

Email: heyi@swjtu.edu.cn

Telephone No: +86 15982104767

Postal address:

No. 111 The Second Circled Road North,

Chengdu, Sichuan, China

610031

Other author's email addresses:

fy980220@swjtu.cn (Y. Fang)

cj1333@my.swjtu.edu.cn (J. Cui)

D.Wan@leeds.ac.uk (D. Wanatowski)

N.Nikitas@leeds.ac.uk (N. Nikitas)

yuanran@swjtu.edu.cn (R. Yuan)

Abstract

Appropriate constitutive models and reliable excavation and support sequences are believed to be the major concern in using Finite element (FE) analysis to simulate shield tunnel excavation. This paper presents systematic 2D and 3D FE analyses employing a number of constitutive models accounting for initial soil anisotropy and non-coaxial plasticity, as evidenced within site investigations from the Tsinghuayuan Tunnel of the Jing-Zhang High-Speed Railway in China. The aim is to assess the effects of both the initial soil anisotropy and non-coaxiality on longitudinal and transverse tunneling-

induced surface settlements. It is shown that the excavation procedures combined with the degree of cross-anisotropy are key towards the accurate prediction of maximum vertical displacements from tunneling, matching field data. Knowledge of the initial soil strength anisotropy can further improve the shape prediction of the transverse tunneling-induced surface settlement troughs. When considering $n = 0.6$ and in simulations, the transverse surface settlement trough obtained is almost coincided with monitored field data. Initial stiffness anisotropy used in the prediction of shield tunnel-induced surface settlements in sandy pebble soils, does improve realism of results significantly. The maximum longitudinal settlement predicted by considering cross-anisotropy is larger than that predicted by its isotropic counterpart.

Keywords: tunneling; surface settlements; FE modelling; constitutive models; soil anisotropy; non-coaxial plasticity

Introduction

Serviceability design of shield tunnels requires accurate estimation of the surface settlements, especially for city areas, where there is existing sensitive infrastructure above the ground (e.g., Ou et al. 1998; Möller 2006; Zhu and Li 2016). Different design methods for serviceability with respect to ground movements have been utilized in engineering, such as simple purely empirical ones, e.g., the Gaussian curve (Martos 1958; Schmidt 1969; Peck 1969); and analytical ones, e.g., the Cavity Expansion (Yu 2000). FE analysis has been also an attractive option, particularly in the past few decades, since it can deal with cases of complex tunnel geometries, complex geological conditions, and can simulate realistically tunneling procedures such as the lining segment installation sequence (as reviewed by Lee and Rowe 1989; Kung et al. 2007; Zhou 2015; Svoboda and Masin 2011). It has been noted by several researchers that the transverse surface settlement trough induced by tunneling obtained from numerical simulations is normally too wide when compared to the field data, especially for the cases of sand or high coefficient of earth pressure at rest (e.g., Gunn 1993; Simpson et al. 1996; Addenbrooke et al. 1997; Franzius 2005). There are two major concerns that should be taken into consideration in such FE approaches, namely the constitutive models for the soil or rock and the excavation and support sequences.

The importance of excavation procedures for tunnels has been emphasized by Möller (2006), who concluded that they are of key importance for arriving at accurate predictions of tunneling settlements. Intuitively expected, tunneling-induced stress redistributions and soil disturbances could be more accurately simulated utilizing three-dimensional (3D) numerical models, rather than 2D ones. On these grounds, many researchers considered 3D analysi to be the obvious way to enhance numerical predictions of tunneling-induced surface settlement troughs (Lee and Ng 2002; Guedes and Santos 2000; Dolezalova 2002; Vermeer et al. 2002; Franzius et al. 2005; Kivi et al. 2012; Mooney et al. 2016; Michael et al. 2017; Hu et al. 2020; Lai et al. 2020, among others). Interestingly their findings refute expectations and 3D FE analyses are shown to not always be better than 2D ones. For real tunnel projects, especially for tunnels with long excavation paths and different cross-sections, 3D FE analyses could be extremely time consuming. Therein, 2D FE analyses could be very useful and could even compensate for the effect of the missing dimension through effective means, such as the stress reduction method, the stiffness reduction method

(Swoboda 1979) and the gap reduction method (Rowe et al. 1983). This is probably why Addenbrooke et al. (1997) used 2D FE analyses to simulate the excavation of the Jubilee Line extension beneath St James's Park in London, UK, and Simpson et al. (1996) performed a 2D FE analysis to simulate the construction of the Heathrow Express trial tunnel in the UK.

In the study of Lee and Ng (2002), who used a linear perfect elastoplastic soil to simulate shield tunneling, the conclusion that 3D modelling resulted in better surface settlement predictions, over 2D, comes challenge the above. Addenbrooke et al. (1997), for instance, through two-dimensional (2D) FE simulations using an isotropic Mohr-Coulomb yield surface to simulate the London clay, predicted a relatively wide surface settlement trough when compared to the field data. Similar conclusions were drawn by Gunn (1993) and Simpson et al. (1996). They used different soil models to obtained predictions closer to reality. Franzius et al. (2005) reviewed the above studies and proposed a series of both 2D and 3D FE numerical analyses of shield tunneling beneath St Jame's Park Greenfield monitoring site, which passed through London clay. However, they concluded that the settlement trough can be improved only when unrealistic material constants of the constitutive models are used. Hence, more advanced constitutive models need non-stop studies for the numerical simulations of tunneling.

More recent experimental research and micro-evidence have uncovered that soil behavior is generally non-coaxial. Non-coaxiality refers to the non-coincidence of the principal axes of stress and plastic strain rate tensors (after Roscoe et al. 1967), and it is apparent in geotechnical cases with severe principal stress rotations, e.g., tidal waves, excavations and seismic loadings (Seed et al. 1989; Sassa and Sekiguchi 1999; Grabe and Clayton 2009). Hollow Cylinder Apparatus (HCA) results, particularly, have demonstrated that non-coaxiality is an important aspect of anisotropy of granular soils (e.g., Yang 2013). Soil particles tend to be aligned in some preferred directions during deposition, which is treated as initial anisotropy and can affect the material properties of granular soils (e.g., shear strength and deformation characteristics). Recently, Yuan et al. (2018a, 2018b) applied their newly proposed constitutive model accounting for non-coaxiality and initial strength anisotropy to perform the 2D plane strain numerical study of tunneling. Normalized shape surface settlement predictions were improved, demonstrating the merits of the newly proposed constitutive models. However, the maximum vertical displacement is still very small.

Although the many studies on the topic, the outcomes are still unsatisfactory, especially when considering the comparison of results with actual field projects. The Tsinghuayuan Tunnel, which is part of the Jing-Zhang High-Speed Railway in Beijing, China; several sections pass through an old urban area in Beijing, where there are many aged buildings with high-risk of failure. Subsurface settlements induced by shield tunneling are easily to cause cracks, or even collapse of the buildings if not being well controlled. Hence accurate estimation of the surface settlements is highly sought. Previous predictions of subsurface settlements from numerical simulations with a Mohr-Coulomb constitutive model proved poor when compared to observed field data. The geological conditions are mainly strata of pebble soils with a mixture of pebble, sand and clay in the area in question. This type of soil is more complex to model, since it is discontinuous and highly anisotropic. Numerical simulations with more advanced soil models were suggested as being a best approach towards dealing with the discrepancy.

LIST OF FIGURES

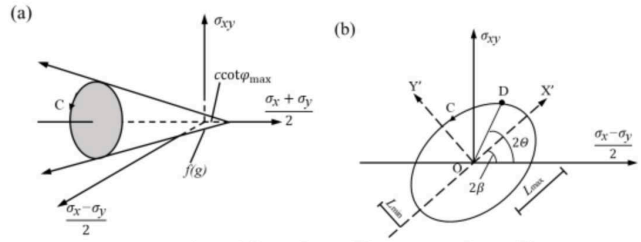

Figure 1. The Mohr-Coulomb yield surface with soil anisotropy in: (a) ($(\sigma_x - \sigma_y)/2$, σ_{xy}, $(\sigma_x + \sigma_y)/2$) space; (b) ($(\sigma_x - \sigma_y)/2$, σ_{xy})space (after Yuan et al (2019)).

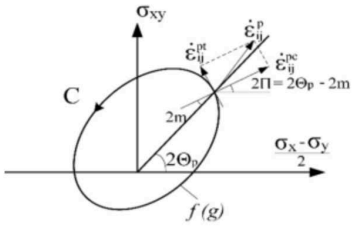

Figure 2. The Mohr-Coulomb yield criterion considering soil anisotropy and non-coaxial plastic flow rule in the ($(\sigma_x - \sigma_y)/2$, σ_{xy}) space (Yuan et al. 2018a, 2018b).

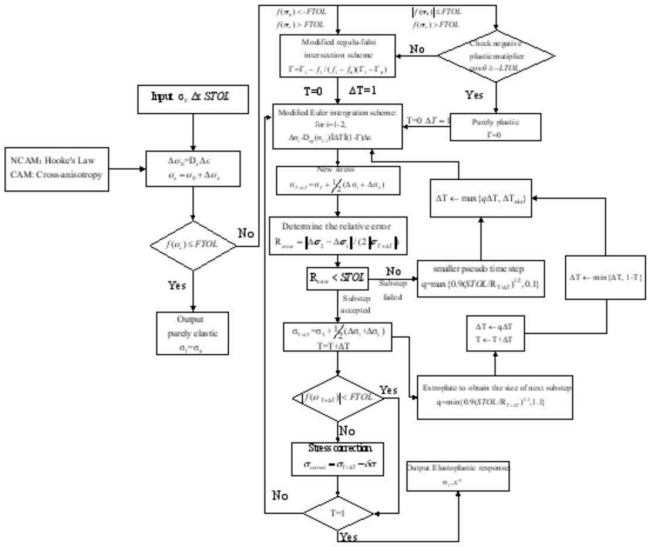

Figure 3. Flowchart of the integration procedure (after Yuan et al (2019).

Figure 4. Plan view of the Tsinghuayuan Tunnel project in Beijing.

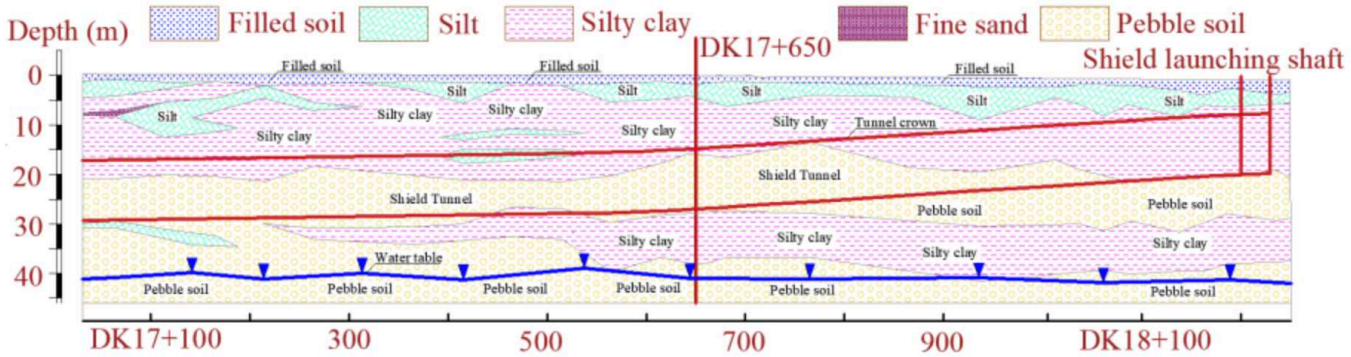

Figure 5. Profile of soil layers and tunnel from DK18+200 to DK17+100.

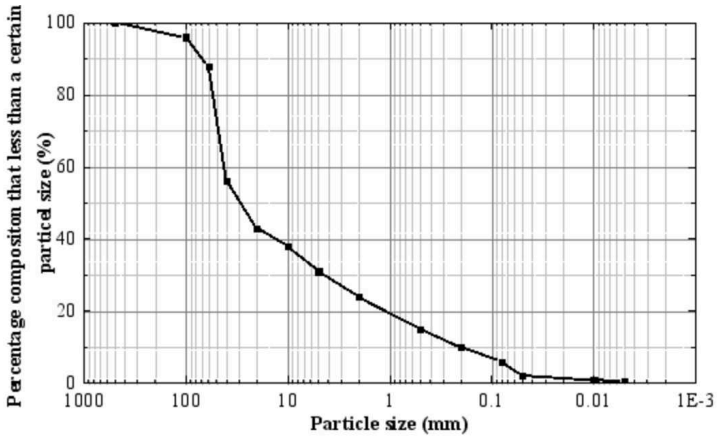

Figure 6. Particle size distribution of the sandy pebble soils near the monitoring section.

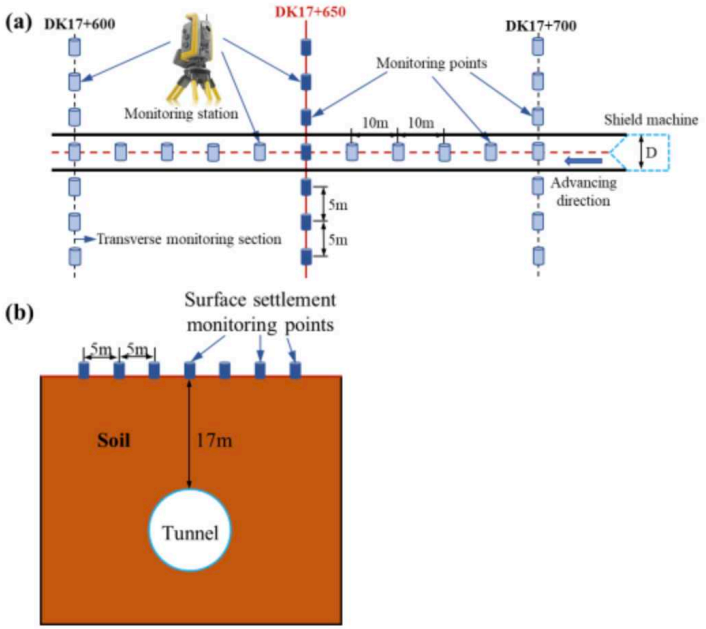

Figure 7. Schematic diagram of monitoring system from DK17+600 to DK17+700: (a) Monitoring system of the transverse surface settlement; (b) Layout of surface settlement monitoring points on the monitoring section DK17+650.

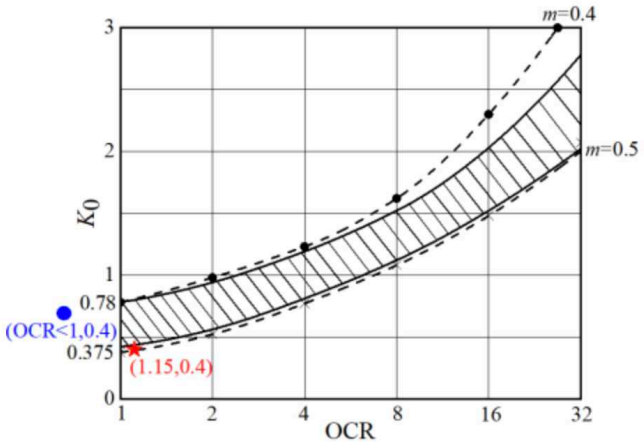

Figure 8. The relationship between K0 and OCR of sandy pebble soil (Based on Li et al. 2013).

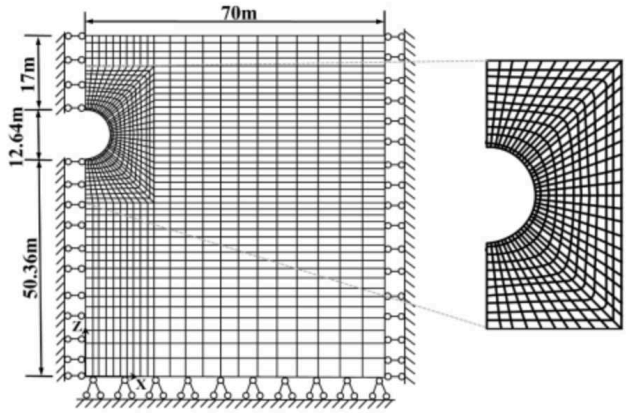

Figure 9. 2D numerical model of the Tsinghuayuan Tunnel.

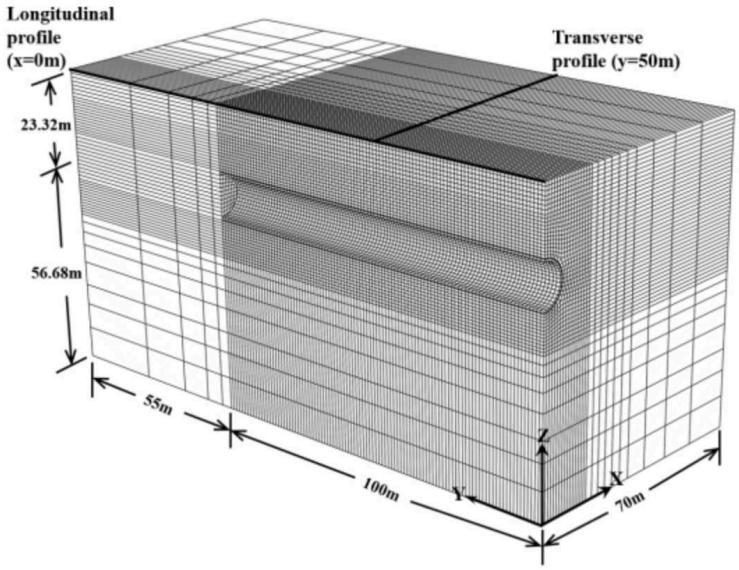

Figure 10. 3D numerical model of the Tsinghuayuan Tunnel (only half of the model is shown).

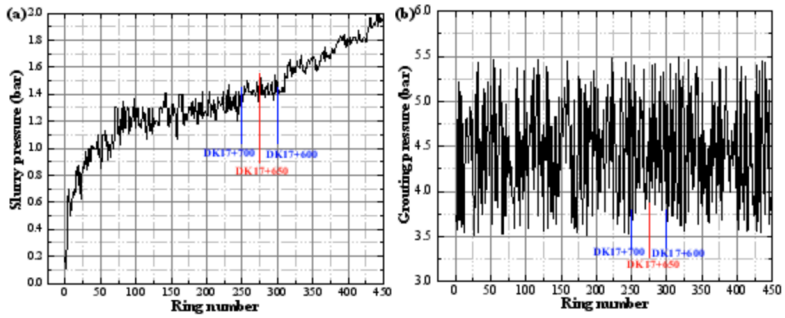

Figure 11. History of slurry and grouting pressures: (a) Slurry pressure; (b) Grouting pressure.

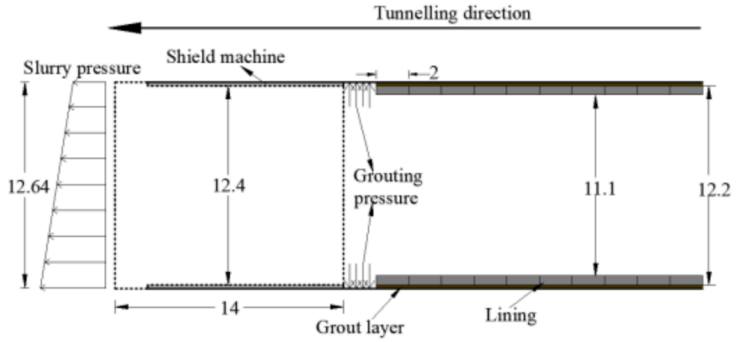

Figure 12. Simulation procedure in 3D numerical model (Units: m).

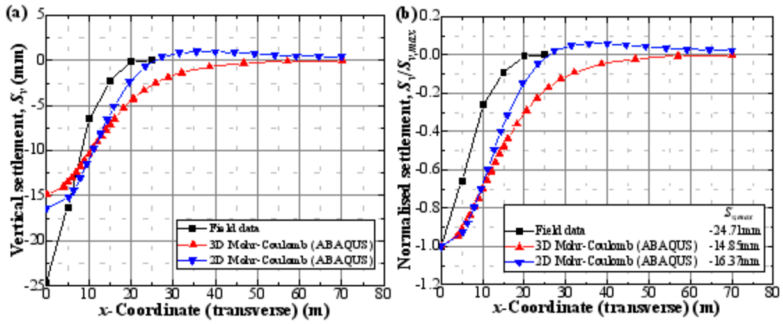

Figure 13. Transverse settlement troughs for 2D and 3D isotropic analyses with field data: (a) Vertical settlement; (b) Normalized settlement.

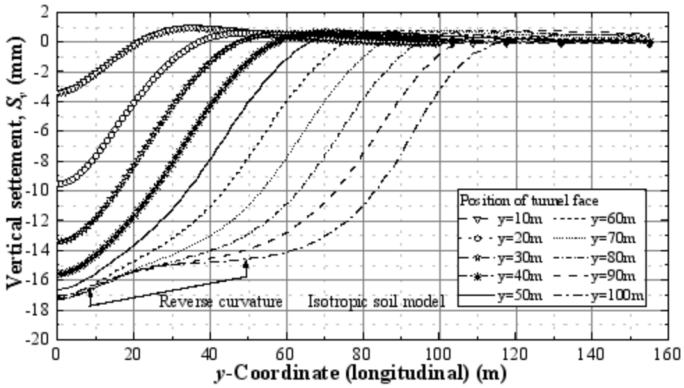

Figure 14. Longitudinal settlement troughs obtained from isotropic 3D simulation analyses.

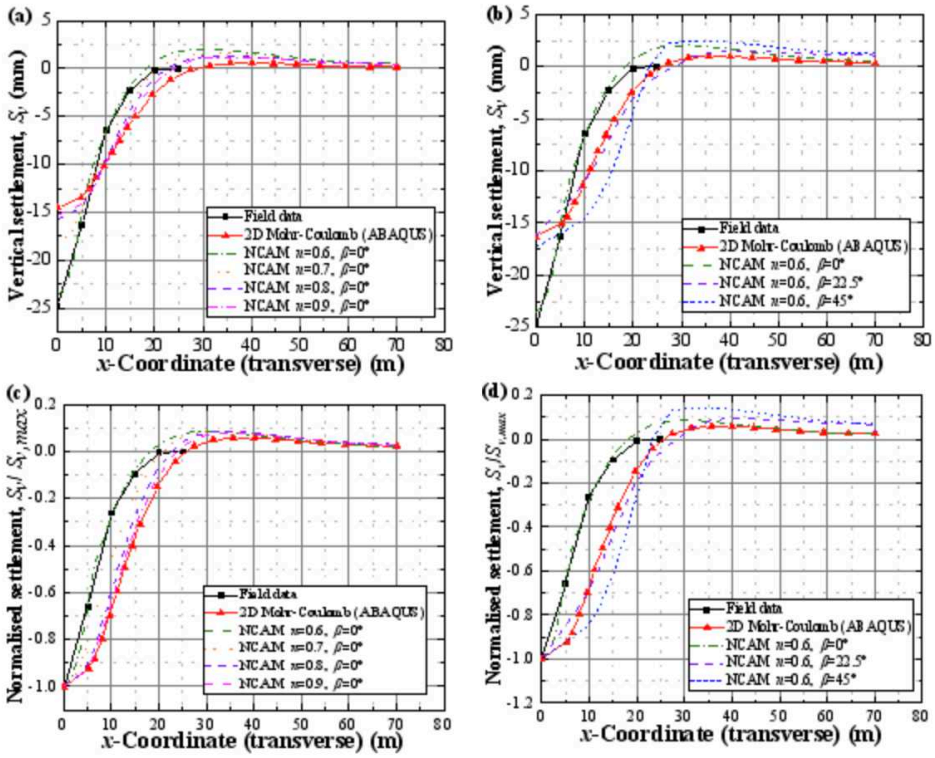

Figure 15. Surface settlements based on anisotropic Mohr-Coulomb yield criterion: (a) Vertical settlement with change of n; (b) Vertical settlement with change of β; (c) Normalized settlement with change of n; (d) Normalized settlement with change of β.

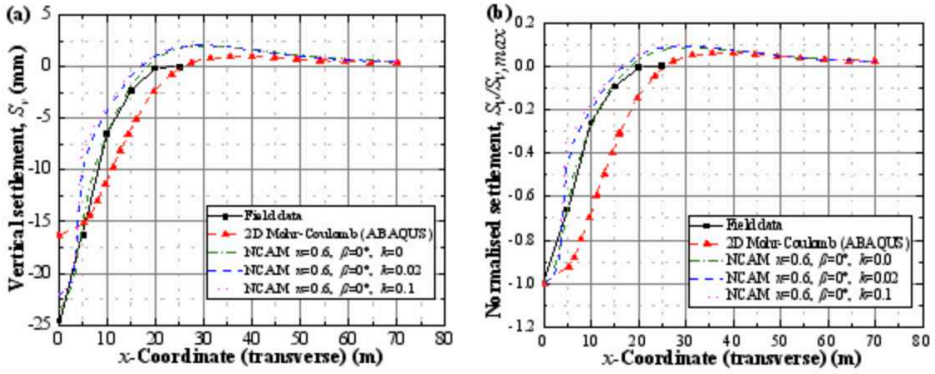

Figure 16. Surface settlements based on anisotropic yield criterion with non-coaxial plastic flow rule: (a) Vertical settlement; (b) Normalized settlement.

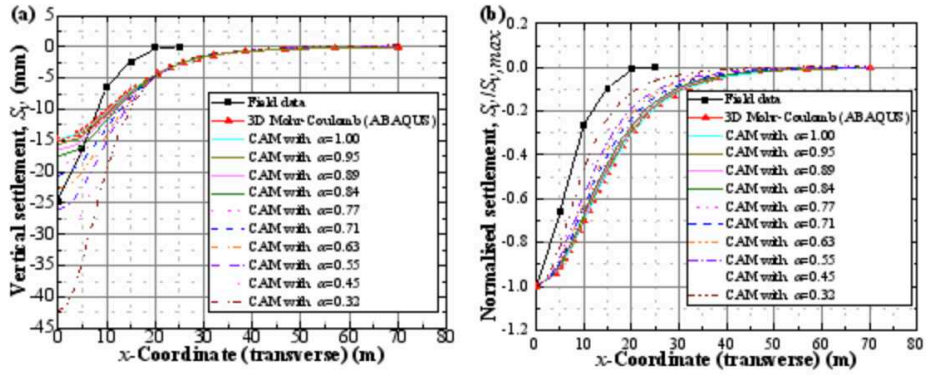

Figure 17. Transverse surface settlement based on cross-anisotropic model in elastic range: (a) Vertical settlement; (b) Normalized settlement.

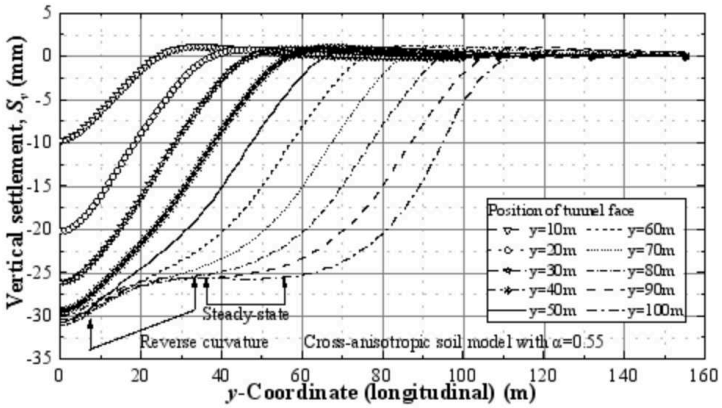

Figure 18. Longitudinal settlement troughs for cross-anisotropic 3D analyses.

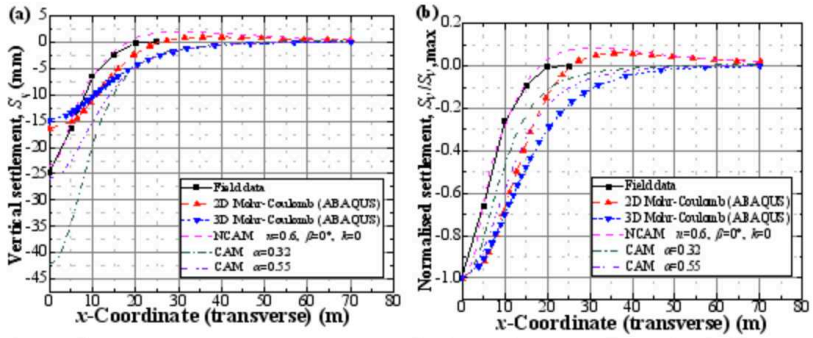

Figure 19. Transverse settlement troughs for isotropic and anisotropic (NCAM and CAM) soil models: (a) Vertical settlement; (b) Normalized settlement.

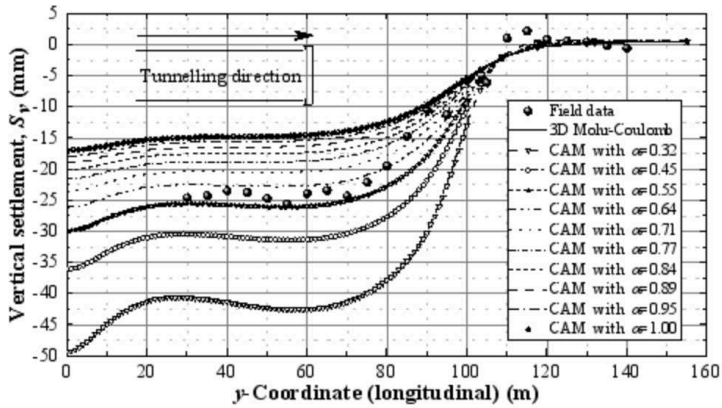

Figure 20. Longitudinal settlement troughs at the end of the tunneling analyses compared with field data.

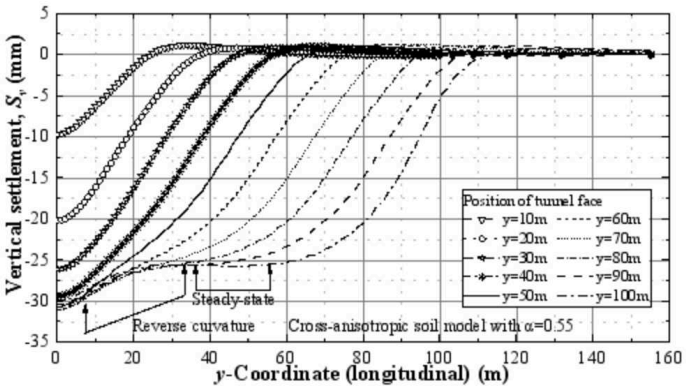

Figure 18. Longitudinal settlement troughs for cross-anisotropic 3D analyses.

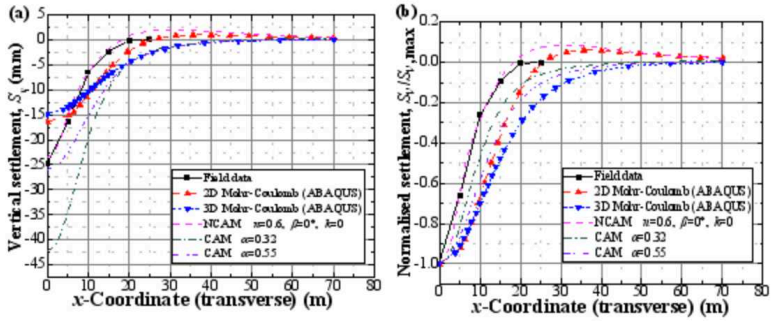

Figure 19. Transverse settlement troughs for isotropic and anisotropic (NCAM and CAM) soil models: (a) Vertical settlement; (b) Normalized settlement.

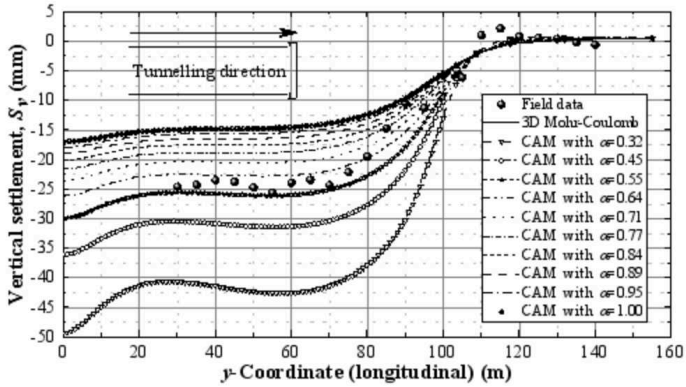

Figure 20. Longitudinal settlement troughs at the end of the tunneling analyses compared with field data.

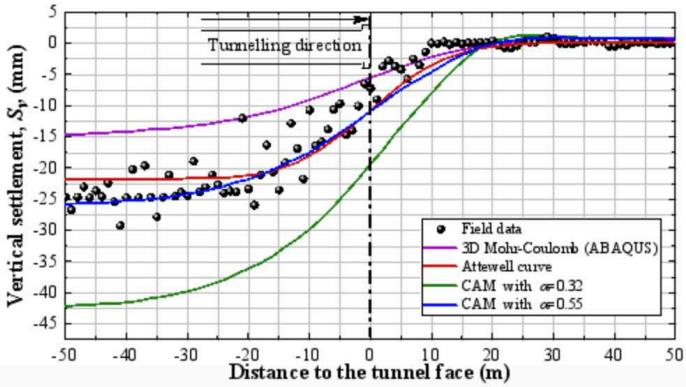

Figure 21. Distribution of surface settlements along the longitudinal direction.

LIST OF TABLES

Table 1. Physical and mechanics parameters of soils by laboratory tests.

Soil		G_s	e	n	S_r		w_L	w_p	I_p	I_L	I_r
Silt	20.5	2.70	0.664	19.9	89.1	1.63	26.3	18.7	8.4	0.31	1.41
Silty clay	22.9	2.72	0.671	20.1	93.0	1.64	31.4	18.5	12.9	0.34	1.70
Sandy pebble soil	23.9	2.71	0.731	20.2	88.6	1.57	29.2	17.6	11.6	0.54	1.66

Note: Units throughout for the properties are shown in notation.

Table 2. Soil material properties for isotropic Mohr-Coulomb yield criterion.

Soil	Bulk density (kN/m³)	Young's modulus (MPa)	Poisson's ratio	Friction angle (°)	Cohesion (kPa)
Sandy pebble soil	20.2	136	0.28	45	1.0

Table 3. Summary of lining, grout layer and shield machine properties.

Specification	Reinforced concrete lining	Backfill grouting		Shield machine
Bulk density (kN/m³)	25	22		76
Young's modulus (MPa)	35500	I- level II- level III- level	4.8 48 200	210000
Poisson's ratio	0.25	0.30		0.20
Thickness (m)	0.55	0.22		0.22

Table 4. Parameters for NCAM simulation.

Case	n	β (°)	k
NCAM-1	0.6	0	0
NCAM-2	0.7	0	0
NCAM-3	0.8	0	0
NCAM-4	0.9	0	0
NCAM-5	1.0	0	0
NCAM-6	0.6	22.5	0
NCAM-7	0.6	45	0
NCAM-8	0.6	0	0.02

NCAM-9	0.6	0	0.1

Table 5. Typical ranges of anisotropic elastic soil constants found in the literature (partial of Jamali et al. 2021).

Measurement no.	Material		v_{vh}	v_h	References
1	London Clay	1.10-2.00	-	-	Ward et al. (1959)
2	Sand	0.30-0.60	-	-	Onas (1970)
3	Clay limestone-Maestrichtian	0.62	-	-	Lozinska-Stepien (1970)
4	Clay limestone- Turonian	0.84-1.69	-	-	Lozinska-Stepien (1970)
5	Opaka marl- Maestrichtian	0.85-1.00	-	-	Lozinska-Stepien (1970)
6	Sandy shale	1.28	0.19	0.10	Stepanov and Batugin (1967)
7	Opaka limestone-Turonian	0.92	-	-	Lozinska-Stepien (1970)
8	Sandstone	1.23	-	-	Stepanov and Batugin (1967)
9	Hard blue slate	1.50	0.43	0.43	Attewell (1970)
10	Bandera sandstone	1.50	0.16	0.14	King (1968)
11	Berea sandstone	1.40	0.22	0.14	King (1968)
12	Aleurolite	1.09	0.26	0.21	Lekhnitskii (1966)
13	Coarse phyllite	1.28	0.33	0.27	Lekhnitskii (1966)
14	Fine phyllite	1.33	0.28	0.26	Lekhnitskii (1966)
15	Sylvinite (rich)	1.13	0.28	0.26	Stepanov and Batugin (1967)
16	Chlorite slate	1.57	0.28	0.17	Stepanov and Batugin (1967)
17	Tuffaceous-sandstone	1.26	0.25	0.02	Stepanov and Batugin (1967)
18	Siltstone	1.08	0.28	0.17	Stepanov and Batugin (1967)
19	“Basalt I”	1.34	0.20	0.11	Stepanov and Batugin (1967)
20	“Basalt II”	1.05	0.14	0.10	Stepanov and Batugin (1967)
21	“Basalt III”	1.08	0.22	0.18	Stepanov and Batugin (1967)
22	Peridotite	1.78	0.32	0.29	Stepanov and Batugin (1967)
23	Barre granite	0.73	-	-	Douglass and Boight (1969)

Table 6. Parameters for CAM simulation.

Case	α	γ	E_h(MPa)	E_v(MPa)	v_h	v_{vh}	G_h(MPa)	G_{vh}(MPa)
CAM-1	1.00	1.0	136.00	136	0.28	0.28	53.13	53.13
CAM-1	0.95	0.9	122.40	136	0.27	0.28	47.81	50.40
CAM-2	0.89	0.8	108.80	136	0.25	0.28	42.50	47.52
CAM-3	0.84	0.7	95.20	136	0.24	0.28	37.19	44.45
CAM-4	0.77	0.6	81.60	136	0.22	0.28	31.88	41.15
CAM-5	0.71	0.5	68.00	136	0.20	0.28	26.56	37.57
CAM-6	0.63	0.4	54.40	136	0.18	0.28	21.25	33.60
CAM-7	0.55	0.3	40.80	136	0.15	0.28	15.94	29.10
CAM-8	0.45	0.2	27.20	136	0.13	0.28	10.63	23.76
CAM-9	0.32	0.1	13.60	136	0.09	0.28	5.31	16.80